Mathematical Monographs
vol. 9 (2016), pp. 65-73

Numerical simulation of fouling by particles in dead-end constant-pressure microfiltration

Kazuki AKAMATSU, Shosuke KANASUGI, Masahiro FUJITA
and Shin-ichi NAKAO

Abstract. Fouling behaviors by particles in dead-end constant- pressure microfiltration processes were numerically simulated using a novel simulator SNAP (Structure of NAnoParticles). The characteristics of the simulation model in SNAP is the use of the two-way coupling method, which considers the effect of particle motion on fluid flow as well as that of fluid flow on particle motion even when the concentration of particles is higher. The simulation studies demonstrated the effect of surface porosity of membrane on the fouling behaviors was much larger than that of particle diameter. And they also demonstrated that the difference in surface porosity resulted in two fouling modes.

1. Introduction

Microfiltration (MF) is one of the fundamental processing techniques for removing particulate substances, and has been used for various fields such as wastewater treatment and food industries. When colloidal suspensions are treated with MF membranes, the particles rejected inside the pores or onto the membrane surfaces increase the resistance for filtration, resulting in the decrease in membrane performances. This fouling phenomenon is the severest issues in membrane processes, and a number of studies for mitigating fouling have been carried out. However, the essential problem that remains unsolved is the fact that no one can understand the fouling dynamics by particles in MF processes. This is mainly because it is almost impossible to observe directly how fouling evolves inside pores and near membrane surfaces. Even though some analytical models describing potential fouling modes were developed [7], they cannot show us anything about the fouling dynamics.

In contrast, many simulation studies have been reported to give us some useful insights in the fouling dynamics because these studies can show us how particles move and how they are trapped during filtration, in particular inside pores. Another advantage in such simulation studies is that we can study the effect of each specific parameter individually, such as membrane pore size and surface porosity, by changing parameter sets. It is also difficult to achieve that experimentally. Most of these studies on fouling by particles in MF use computational fluid dynamics (CFD). In such CFD simulations, the flow field is first calculated and then the motion of particles are treated by making the particles trace along the streamlines, which means that the effect of fluid flow on particle motion is simply considered but that

the effect of particle motion on fluid flow and the effect of particle motion on other particles motions are not considered. Fouling occurs near the membrane surface and inside the pores, where particles are expected to be much concentrated. Thus all the effects mentioned above should be included, and these conventional simulation studies should be improved for further understandings of the fouling dynamics. Fujita and Yamaguchi developed a new class of simulators, SNAP (Structure of NAnoParticles), which includes all the effects [3-6], and Ando et al extended these simulators to demonstrate fouling and backwash dynamics in dead-end, constant-pressure MF processes [1-2]. These simulation studies compensate for shortcomings of the conventional studies using CFD, and can precisely simulate both the fluid flow and the particles motions near membrane surface and inside pores where particles are concentrated. And they will exactly lead to our understandings of fouling dynamics.

Here we report the simulation studies on the effects of particle size and surface porosity on fouling behaviors in dead-end constant-pressure MF processes using SNAP.

2. Simulation model

2.1. Flow of solvent

The fluctuating Navier-Stokes equation is used for the momentum equation of the suspension flow consisting of particles and water.

$$\frac{\partial \mathbf{v}}{\partial t} + (\mathbf{v}\cdot\nabla)\mathbf{v} = -\frac{1}{\rho}\nabla p + \frac{\mu}{\rho}\nabla^2\mathbf{v} + \frac{1}{\rho}\nabla\cdot\mathbf{S} - \frac{1}{\rho}\mathbf{D} + \Phi\boldsymbol{\alpha} \tag{1}$$

$$\boldsymbol{\alpha} = \frac{\mathbf{v}^p - \mathbf{v}}{\Delta t} + (\mathbf{v}\cdot\nabla)\mathbf{v} - \frac{\mu}{\rho}\nabla^2\mathbf{v} - \frac{1}{\rho}\nabla\cdot\mathbf{S} + \frac{1}{\rho}\mathbf{D} \tag{2}$$

$$\nabla\cdot\mathbf{v} = 0 \tag{3}$$

where t is time, $\mathbf{v}$ is the fluid velocity vector on the computational lattice, ρ is the density of the solvent, p is the pressure, μ is the viscosity of the solvent, and $\mathbf{D}$ is the pressure gradient vector. $\mathbf{S}$ is the thermal fluctuating stress tensor for incompressible flows [5], and expressed as following.

$$\langle \boldsymbol{S}_{ij}(\boldsymbol{r},t)\rangle = 0$$

$$\langle \boldsymbol{S}_{ik}(\boldsymbol{r},t)\boldsymbol{S}_{lm}(\boldsymbol{r}',t')\rangle = 2k_{\mathrm{b}}T\mu(\delta_{il}\delta_{km} + \delta_{im}\delta_{kl})\delta(\boldsymbol{r}-\boldsymbol{r}')\delta(t-t') \tag{4}$$

where, $\langle\ \ \rangle$ denotes an ensemble average, k_{b} is Boltzmann constant, δ_{ij} is the Kronecker's delta, and $\delta(\ \ )$ is the Dirac delta function. In three dimensions, Eq.(4) is written as

$$\langle s_{xx}\rangle = \langle s_{xy}\rangle = \langle s_{xz}\rangle = \langle s_{yx}\rangle = \langle s_{yy}\rangle = \langle s_{yz}\rangle = \langle s_{zx}\rangle = \langle s_{zy}\rangle = \langle s_{zz}\rangle = 0$$

$$\langle {s_{xx}}^2\rangle = \langle {s_{yy}}^2\rangle = \langle {s_{zz}}^2\rangle = 4k_{\mathrm{b}}T\mu\delta(x-x')\delta(y-y')\delta(z-z')\delta(t-t')$$

$$\langle {s_{xy}}^2\rangle = \langle {s_{yx}}^2\rangle = \langle {s_{yz}}^2\rangle = \langle {s_{zy}}^2\rangle = \langle {s_{xz}}^2\rangle = \langle {s_{zx}}^2\rangle$$

$$= 2k_{\mathrm{b}}T\mu\delta(x-x')\delta(y-y')\delta(z-z')\delta(t-t') \tag{5}$$

Φ is the volume fraction of particles and membrane on the computational lattice, ranging from 0 (outside a particle) to 1 (inside a particle). $\boldsymbol{\alpha}$ is the acceleration vector associated with the rigid velocity of particles on the lattice. Here we handle the membrane in the same method as particles. The velocity of the membrane is fortified as zero. The finite difference method was employed to solve these equations, and based on the immersed boundary method the combination of the flow of solvent and the motion of particles are integrated.

2.2. Motion of particles

A Newton's equation of motion is used for the motion of particles. The translational motion of the *l*-th particle is expressed as follows

$$m_l \frac{d\boldsymbol{V}_l}{dt} = \boldsymbol{F}_l^c + \boldsymbol{F}_l^e + \boldsymbol{F}_l^v + \boldsymbol{F}_l^h + \boldsymbol{F}_l^{lb} \tag{6}$$

where m_l is the mass of the particle, $\boldsymbol{V}_l$ is the translational velocity vector of the particle, and $\boldsymbol{F}_l^c$, $\boldsymbol{F}_l^e$, $\boldsymbol{F}_l^v$, $\boldsymbol{F}_l^h$ and $\boldsymbol{F}_l^{lb}$ are the contact force, the electrostatic force, the van der Waals force, the hydrodynamic force, and the lubrication force, respectively [1,4]. $\boldsymbol{F}_l^c$ is expressed by the following equation.

$$\boldsymbol{F}_l^c = \sum_m (\boldsymbol{F}_{lm}^{\mathrm{n}} + \boldsymbol{F}_{lm}^{\mathrm{t}}) \tag{7}$$

$\boldsymbol{F}_{lm}^{\mathrm{n}}$ and $\boldsymbol{F}_{lm}^{\mathrm{t}}$ are normal contact force and tangential contact force at the contact point of the *l*-th particle and *m*-th particle, respectively.

The rotational motion of the *l*-th particle is expressed as follows

$$I_l \frac{d\boldsymbol{\omega}_l}{dt} = \boldsymbol{T}_l^c + \boldsymbol{T}_l^h \tag{8}$$

where I_l is the moment of inertia of the particle, $\boldsymbol{\omega}_l$ is the angular velocity vector of the particle, and $\boldsymbol{T}_l^c$ and $\boldsymbol{T}_l^h$ are the contact torque and the hydrodynamic torque, respectively. The hydrodynamic force $\boldsymbol{F}_l^h$ and torque $\boldsymbol{T}_l^h$ acting on the *l*-th particle are expressed by the following equations.

$$\boldsymbol{F}_l^h = -\int_{V^p} \varphi_l(\boldsymbol{r})\{\rho\boldsymbol{\alpha}(\boldsymbol{r}) + \mathbf{D}\} dV \tag{9}$$

$$\boldsymbol{T}_l^h = -\int_{V^p} \varphi_l(\boldsymbol{r})\{\boldsymbol{r}_l(\boldsymbol{r}) \times \rho\boldsymbol{\alpha}(\boldsymbol{r})\} dV \tag{10}$$

where V^p is the region occupied by the *l*-th particle, φ_l is the volume fraction of the *l*-th particle, whose sum is Φ. $\boldsymbol{r}_l$ is the position vector relative to the spherical center of the *l*-th particle. The diffusion of particles is obtained through $\boldsymbol{F}_l^h$ and $\boldsymbol{T}_l^h$, including the stochastic fluctuating stress [2].

2.3. Simulation method and condition

In this study, the equations for the motions of particles are solved using the first-order Euler explicit scheme, and the equation for particle position is solved

using the Crank-Nicolson scheme. Then the fluctuating Navier-Stokes equation is solved using the two-step method. The first step utilizes the semi-implicit method for pressure-linked equations shortened (SIMPLEST) [8], and the second step uses the convergence algorithm by the iterative calculation of pressure [2].

Table 1 summarizes the simulation condition. Each particle is spherical, with a diameter d (50, 150, 200 nm). Particle is shot one by one to maintain the concentration of particles in feed to be 1 vol%. The computational domain is shown in Figure 1, representing a simple three-dimensional channel. A periodic boundary condition on the faces parallel to the direction of flow is used. The domain of x is fixed to 18d, and those of y and z are changed to tune the surface porosity under the condition where y is equal to z. The surface porosity is defined as follows

$$\varphi_{\mathrm{p}} = \frac{\pi\left(d^{m}/_{2}\right)^{2}}{yz} \times 100 \tag{11}$$

The membrane has a thickness of 6d, located at the center of the domain, and has a single, straight cylindrical pore at the center with a pore size d^{m} (d / d^{m} = 0.5). The pressure gradient is adjusted to obtain 1 m^3 m^{-2} s^{-1} initial permeate flux. The lattice spacing of the flow field is 1/9d.

Table 1. Simulation conditions

	Nomenclature	Value
Particle	Diameter, d [m]	$50, 150, 200 \times 10^{-9}$
	Density, ρ^{p} [kg m^{-3}]	3.15×10^{3}
	Young's modulus, E^{p} [Pa]	3.83×10^{9}
	Poisson ratio [-]	0.34
	Friction coefficient between particles, η^{p} [-]	0.1
	Friction coefficient between particle and membrane, η^{m} [-]	0.1
	Zeta potential, Ψ^{p} [mV]	-40
	Concentration, φ_{v} [vol%]	1
	Hamaker constant, A [J]	8.3×10^{-19}
Solvent	Density, ρ [kg m^{-3}]	9.98×10^{2}
	Viscosity, μ [Pa s]	1.0×10^{-3}
	Relative permittivity, ε_{r} [-]	8.02×10^{1}
	Ionic strength of the electrolyte [mol L^{-1}]	1.0×10^{-4}
	Valence of ions [-]	1

	Temperature, T [K]	298.15
Membrane	Thickness, t^m [m]	$6 \times d$
	Surface porosity, φ_p [%]	12.6 , 19.6, 34.9%
	d/d^m [-]	0. 5
	Young's modulus, E^m [Pa]	3.83×10^9
	Poisson ratio [-]	0.34
	Zeta potential, Ψ^m [mV]	-40
	Hamaker constant, A^m [J]	8.3×10^{-19}

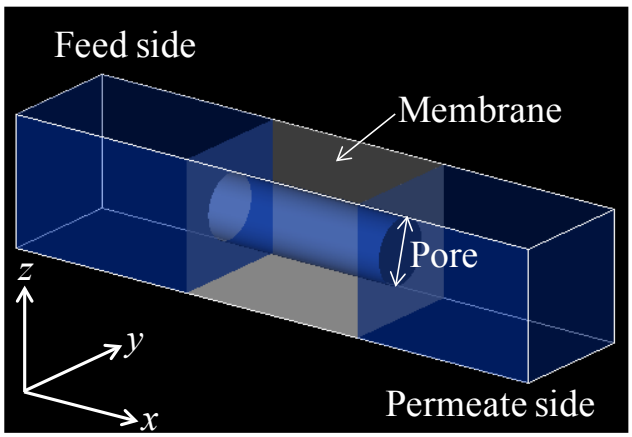

Figure 1. The computational domain for dead-end constant-pressure microfiltration

3. Results and discussion

Figure 2 shows the flux profiles with a function of the ratio of total volume of permeate (V_{total}) to pore volume (V_{pore}) when the surface porosity is 34.9% and d ranges from 50 nm to 200 nm. The value of V_{total} / V_{pore} is proportional to the total number of particles that have approached one pore on the front surface, so this comparison makes it possible to discuss potentially how fouling occurs. Regardless of particle diameter tested here, the flux drastically decreased from its initial

1 m^3 m^{-2} s^{-1} to less than 0.2 m^3 m^{-2} s^{-1}. During these flux drops, particles rejected by the membrane became the resistance for filtration. Figure 3(a)-(c) show the final snapshot for each simulation. The pore was clogged by the rejected particles in all

cases. The clogging was first observed at the back surface of the membrane. After that, all particles pass through the pore entrance and were rejected inside the pore. Consequently, the clogging layer grew up from the back to the front within the pore.

Though no effect of the particle diameter on the flux profile and fouling dynamics was observed in the case of 34.9% of surface porosity, another fouling mode was observed when the surface porosity of the membrane was 12.6% and 19.6%. In these cases, the fouling by the rejected particles also occurred, however the filtration resistance was formed at the front surface of the membrane. The particles are rejected at the front and pile up to form the cake layer, which is often seen in the practical MF operation. This phenomenon was also independent of the particle diameter tested in this study.

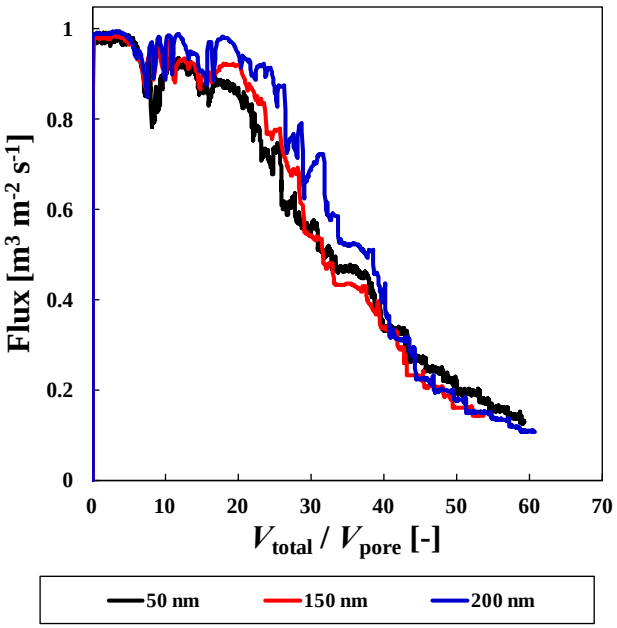

Figure 2. The flux profiles with a function of V_{total} / V_{pore}.
The particle diameter ranges from 50 nm to 200 nm.

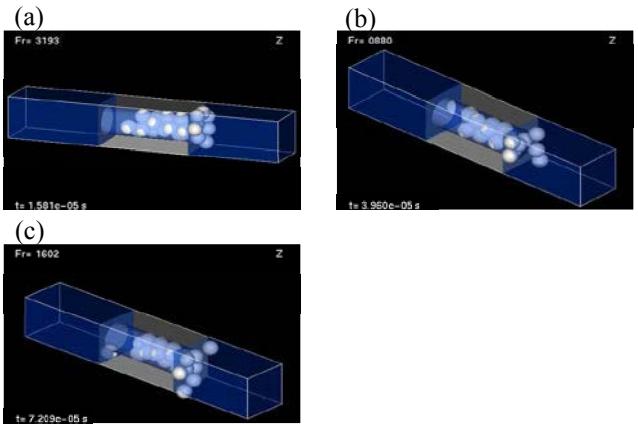

Figure 3. The final snapshot for (a) d = 50 nm, (b) d = 150 nm, (c) d = 200 nm.

The effects of the particle diameter (d) and the surface porosity on the fouling modes are summarized in Table 2. "Cake" means the fouling mode in which the pore entrance at the front surface is covered by particles, and where a cake layer subsequently forms. "Clogging" means the fouling mode in which particles can pass through the pore entrance but are then trapped at the back face, so that pore clogging progresses from the back toward the front by subsequent particles that enter the membrane at the front surface and become trapped. The fouling mode was strongly affected by the surface porosity, not by the particle diameter. In the simulation condition, d, d/d^m, particle concentration and the initial flux are fixed, so the surface density of particles per certain time for each pore would be inversely proportional to surface porosity in the early stages of MF. Smaller surface porosity then results in a crowded condition at each pore entrance on the front surface, and this concentrated state induces collision and coverage of each pore. Subsequently, the fouling mode becomes "Cake" mode. Otherwise, particles can easily enter the pore. And then some of the particles are trapped at the back surface of the membrane, and "Clogging" mode occurs.

Table 2. Fouling mode affected by the particle diameter and the surface porosity

		Surface porosity [%]		
		12.6	19.6	34.9
Particle diameter [nm]	50	Cake	Cake	Clogging
	150	Cake	Cake	Clogging
	200	Cake	Cake	Clogging

4. Conclusions

In this study, numerical simulation of fouling caused by particles was carried out under different particle diameter and different surface porosity of the membrane with SNAP simulator employing the two-way coupling method, which means that both the effect of particle motion on fluid flow and that of fluid flow on particle motion are precisely considered. The effect of particle diameter on the fouling behavior was much smaller than that of surface porosity, and the difference in the surface porosity resulted in two fouling mode. One is "Clogging" mode, and the pore is clogged from the back surface of the membrane. The other is "Cake" mode, and the cake layer is formed from the front surface of the membrane. This can be explained by the relationship between the surface porosity and the concentrated condition near the pore entrance.

There remain many parameters that would affect the fouling behaviors, such as zeta potentials of particles and membranes, pore structures. Further studies are required for better understandings of fouling phenomena caused by particles in MF processes.

References

[1] Ando, T., Akamatsu, K., Fujita, M. and Nakao, S. (2010). Direct simulation model of concentrated particulate flow in pressure-driven dead-end microfiltration, *Journal of Chemical Engineering of Japan*, **43**, 815-828.

[2] Ando, T., Akamatsu, K., Nakao, S. and Fujita, M. (2012) Simulation of fouling and backwash dynamics in dead-end microfiltration: Effect of pore size, *Journal of Membrane Science*, **392-393**, 48-57.

[3] Fujita, M. and Yamaguchi, Y. (2006). Development of three-dimensional structure formation simulator of colloidal nanoparticles during drying, *Journal of Chemical Engineering of Japan*, **39**, 83-89.

[4] Fujita, M. and Yamaguchi, Y. (2007). Multiscale simulation method for self-organization of nanoparticles in dense suspension, *Journal of Computational Physics*, **223**, 108-120.

[5] Fujita, M. and Yamaguchi, Y. (2008). Simulation model of concentrated colloidal nanoparticulate flows, *Physical Review E*, **77**, 026706.

[6] Fujita, M., Koike, O. and Yamaguchi, Y. (2015). Direct simulation of drying colloidal suspension on substrate using immersed free surface model, *Journal of Computational Physics*, **281**, 421-448.

[7] Grace, H. P. (1956). Structure and performance of filter media. 2. Peformance of filter media in liquid service, *AIChE Journal*, **2**, 316-336.

[8] Spalding, D. B. (1981). A general purpose computer program for multi-dimensional one- and two-phase flow, *Mathematics and Computers in Simulation*, **23**, 267-276.

Kazuki Akamatsu, Shosuke Kanasugi and Shin-ichi Nakao

Department of Environmental Chemistry and Chemical Engineering, School of Advanced Engineering, Kogakuin University,
2665-1 Nakano-machi, Hachioji-shi, Tokyo 192-0015, Japan.
akamatsu@cc.kogakuin.ac.jp

Masahiro Fujita
Department of Mathematics, Faculty of Science, Josai University,
2-3-20 Hirakawa-cho, Chiyoda-ku, Tokyo 102-0093, Japan
fujita@josai.ac.jp